

TWENTY-FIFTH EUROPEAN ROTORCRAFT FORUM

Paper no. H7

HIGH-RESOLUTION WAKE MODELLING
IN
HELICOPTER FLIGHT MECHANICS

BY

R.E. BROWN & S.S. HOUSTON
Department of Aerospace Engineering
University of Glasgow
Scotland, UK

SEPTEMBER 14-16, 1999

ROME
ITALY

ASSOCIAZIONE INDUSTRIE PER L'AEROSPAZIO, I SISTEMI E LA DIFESA
ASSOCIAZIONE ITALIANA DI AERONAUTICA ED ASTRONAUTICA



High-Resolution Wake Modelling in Helicopter Flight Mechanics

R.E. Brown and S.S. Houston, Dept. of Aerospace Engineering,
University of Glasgow, Scotland.

We examine the influence of real wake effects, such as blade-vortex and main rotor - tail rotor interaction, on the prediction of the flight dynamic behaviour of rotorcraft by comparing predictions of trim states and stability derivatives by a rigid blade-fuselage model using a Peters-type dynamic inflow model and a new CFD-based wake model. The general similarity of predictions, together with observed differences in certain key cases, suggests that incorporation of real wake effects is important, but that a rigid-blade rotor dynamic model may not be sensitive enough to allow such effects to be fully evident in simulations.

1 Introduction

The overall objective of the work presented here is to examine the significance of aerodynamic effects induced by the detailed structure of the rotor wake on the prediction of the flight dynamic behaviour of rotorcraft.

The current generation of flight dynamic models almost universally use an implementation of Peters' finite-state dynamic inflow formalism¹ to model the effects of the rotor wake on the aerodynamic loading on the rotor. The dynamic inflow approach yields impressive correlation with the available experimental data in most flight regimes, but in important cases such as pitch-roll cross-coupling, heave dynamics and quartering flight the predictions can be disappointing. A significant body of experimental^{2,3} and numerical⁴ work has helped to tentatively isolate the absence of a detailed account of the interactions between the rotors and vortical structures in the wake as the principal reason for the failure of the predictive capability of flight dynamics models based on the dynamic inflow formalism.

In this paper we present representative trim states and stability and control derivatives calculated for the AS330 Puma helicopter using a coupled blade-fuselage flight dynamic model in an attempt to explore some of the effects of detailed modelling of blade-wake aerodynamic interactions on the predictive capability of rotorcraft flight dynamic models. Results calculated using the Peters-HaQuang⁵ dynamic inflow model are contrasted with results obtained using a new wake model⁶ which is based on the numerical solution of the unsteady vorticity transport equations in the neighbourhood of the rotorcraft. This new wake model is constructed with special attention to the generation of detailed wake geometries in as physically rigorous a manner as possible, with minimal assumptions as to the intrinsic structure of the time-evolving wake.

2 Mathematical Modelling

We adopt a relatively standard rotor-fuselage model, structured to allow selection of either the Peters-HaQuang⁵ dynamic inflow model or the new vorticity transport model, described in §2.2, to predict the local velocity at each of the blade elements.

2.1 Blade-Fuselage Model

The coupled blade-fuselage flight dynamic model used in the current investigation employs a blade-element approach to calculate the aerodynamic and inertial loads on each individual blade of the helicopter. These loads are transferred to the airframe via a rigid-blade model with flap and lag degrees of freedom. The resulting equations of motion⁷ are then integrated in state-vector form to obtain the unsteady motion of the rotorcraft. Trim in steady flight is achieved by successive approximation to a state in which the mean forces and moments on the airframe are zero over a period which is long compared to the main rotor's rotational period.⁷ The blade-fuselage model has been used previously for helicopter validation and simulation studies^{7,8} and for the simulation of autogyros.⁹ Further properties of the model are summarised in Table 1.

Rotor dynamics (each rotor)	<ul style="list-style-type: none">• up to ten individually-modelled rigid blades• fully-coupled flap, lag and feather motion• blade attachment by offset hinges and springs• linear lag damper
Rotor loads	<ul style="list-style-type: none">• aerodynamic and inertial loads represented by up to ten elements per blade
Blade aerodynamics	<ul style="list-style-type: none">• lookup tables for lift and drag as function of angle of attack and Mach number
Transmission	<ul style="list-style-type: none">• coupled rotorspeed and engine dynamics• up to three engines• geared or independently-controlled rotor torque
Airframe	<ul style="list-style-type: none">• fuselage, tailplane and fin aerodynamics by lookup tables or polynomial functions
Atmosphere	<ul style="list-style-type: none">• International Standard Atmosphere• provision for variation of sea-level temperature and pressure

2.2 Vorticity Transport Model

Modelling techniques which, at least in principle, are capable of yielding sufficiently detailed predictions of real flow effects such as blade-vortex interactions have been developed in the context of rotor dynamics and loads prediction. Unfortunately, a fundamental mismatch between the timescales associated with the body dynamics and with the rotor modes usually implies that a technique which is detailed enough for rotor dynamic calculations will be computationally prohibitive when applied to flight dynamic analyses. The new wake model solves the unsteady Navier-Stokes equations, reduced by assumptions of zero viscosity and incompressibility to vorticity transport form, on a computational grid enclosing the rotorcraft. The approach adopted here can be specifically optimised for flight dynamics calculations: loss of accuracy and the computational intractability induced by the mismatch between rotor and body timescales is avoided by using a vorticity-conserving formalism and

time-factorisation of the rotor-generated vorticity source into the computational domain. In addition, the characteristic tendency of grid-based methods to over-diffuse any vortical structure present in the flow is addressed by using a Riemann-problem based solver with flux-limiting functions to control spreading during the convection of the vorticity in the wake.

2.2.1 Theoretical Basis

Let V be the volume occupied by the vehicle and its surrounding flow field. Define the vorticity $\omega(\mathbf{x}, t)$ at \mathbf{x} in V in terms of the velocity $v(\mathbf{x}, t)$ of the flow as

$$\omega = \nabla \times v \quad (1)$$

Assuming incompressibility, a Poisson equation

$$\nabla^2 v = -\nabla \times \omega \quad (2)$$

relates the velocity and vorticity of the flow. Adopt the classical, asymptotically inviscid, aerodynamic approach that, at any time t , the generation of aerodynamic forces occurs in some subset $B(t)$ of V while in the remainder of V the flow behaves in an essentially inviscid manner. The Navier-Stokes equations governing the flow in V then reduce to the unsteady vorticity transport equation

$$\frac{\partial}{\partial t} \omega + v \cdot \nabla \omega - \omega \cdot \nabla v = S \quad (3)$$

The source term S is non-zero only in $B(t)$ and the dynamics of the airframe and rotor enters the computation only through the dependence of the source term on the state vector $\mathbf{x}(t)$ describing the loading on, and the subsequent motions of, the airframe and rotors. The analysis of the flow in V is thus decomposed into an outer, wake evolution, problem and an inner problem involving the generation of the aerodynamic forces on the vehicle. The mismatch in timescales in the flight dynamic problem appears in this formulation purely as a mismatch between the timescale associated with the evolution of ω in the absence of sources, and the timescale associated with the evolution of $\mathbf{x}(t)$ and thus S .

2.2.2 Numerical Implementation

Construct a computational domain V' placed so that it surrounds the aircraft and partially encloses the flow in which the vehicle is immersed. Tessellate V' by a finite number N of three-dimensional cells V'_i . A form of Eq. 3 which explicitly expresses the conservation of vorticity follows in standard fashion by piecewise integration over the cellular structure of V' :

$$[\omega]^{n+1} - [\omega]^n = [v \cdot \nabla \omega]_{\Delta t}^n + [S]_{\Delta t}^n - [\omega \cdot \nabla v]_{\Delta t}^n \quad (4)$$

where, for any flow variable $q(\mathbf{x}, t)$,

$$[q]^n = \int_{V'_i} q(\mathbf{x}, n\Delta t) dx \quad \text{and} \quad [q]_{\Delta t}^n = \int_n^{(n+1)\Delta t} [q]^n dt \quad (5)$$

on discretising time as $t = n\Delta t$, $n = 0, 1, \dots$

Given the initial vorticity distribution $[\omega]^0$ in the wake, the sequence $[\omega]^n$, $n = 1, 2, \dots$, generated by the explicit procedure

$$\begin{aligned} v^n &= v * [\omega]^n \\ [\omega]^* &= [\omega]^n + [v \cdot \nabla \omega]_{\Delta t}^n - [\omega \cdot \nabla v]_{\Delta t}^n \\ [\omega]^{n+1} &= [\omega]^* + [S]_{\Delta t}^n \end{aligned} \quad (6)$$

assuming all terms to be dependent only on v^n , $[\omega]^n$ and $\mathbf{x}(t)$, yields an order Δt^2 time-accurate approximation¹⁰ to the vorticity obtained from Eq. 4, provided that the various operators comprising this procedure are all themselves at least second order time-accurate approximations to the operators in Eq. 4. Most importantly, this procedure is stable if each of the operators is allowed to advance within its own particular stability limit.¹⁰

The operator $v * [\omega]^n$ yields an approximation to the solution v of Eq. 2, in the present implementation calculated using a Poisson solver based on Schumann and Sweet's¹¹ method of cyclic reduction. This approach is significantly faster than evaluation of the operator via the Biot-Savart integral, and yields similar computational times to the fast-multipole techniques¹² used in modern Lagrangian wake models. The stretching operator $[\omega \cdot \nabla v]_{\Delta t}^n$ is then approximated by Runge-Kutta integration over a single computational timestep.

The present implementation uses Toro's¹³ Weighted Average Flux (WAF) method, extended to three dimensions using the standard Strang spatial splitting,¹⁴ to approximate the transport operator $[v \cdot \nabla \omega]_{\Delta t}^n$. The WAF method is a conservative Riemann problem-based method which can be modified to use flux limiter functions to create solutions which preserve the monotonicity of $[\omega]^n$ at each timestep. Although the technique was developed to enable the accurate resolution of discontinuities in compressible flows, here the use of flux limiter functions in a conservative formulation allows the compactness of the domains of vorticity in the flow field to be controlled while still conserving the total vorticity present in the computational domain.⁶

The effect on vorticity confinement of using this approach is shown in Figure 1, where the vorticity transport model is used to calculate the wake structure of a three-bladed propeller, advancing axially at 0.35 times its blade tip-speed. A surface of constant vorticity magnitude is plotted to resolve only the structure of the tip vortices. The first diagram, obtained using the mildly-compressive MIN-type limiter,¹⁵ is typical of results obtained using grid-based numerical methods with the second-order time-accuracy of the approach described here. The improvement shown in the second diagram results from replacing the MIN-limiter with a highly-compressive SUPER-type limiter.¹⁵ The success of the present approach at maintaining the strength of the tip vortices all the way to the edge of the computational domain, and, indeed, in confining the vorticity down to the minimum scale resolveable by the computational grid, is evident.

The mismatch of timescales inherent in the flight dynamic problem results in the timestep required to maintain the accuracy and stability of $\mathbf{x}(t)$ generally being very much smaller than the timestep Δt at which Eq. 6 can be advanced in the absence of vorticity sources. The impact of this stiffness on the execution time of the algorithm can be reduced by modifying the structure of the source term to effectively decouple the rate of advance of the inner and outer problems as follows. The conservative structure of Eq. 6 allows the vorticity source to be approximated as $[S]_{\Delta t}^{n*} = [S]_M^{n*}$ on defining a sequence of intermediate sources of vorticity

$$[S]_m^{n*} = [S]_{m-1}^{n*} + [S]_{\Delta t/M}^{n+m/M} (\mathbf{x}(n\Delta t + m\Delta t/M) , v^n + v_m^*) \quad (7)$$

if $0 < m \leq M$, on defining $[S]_0^{n*} = 0$, and where v_m^* is a correction to the velocity field to account for the source of vorticity during intermediate steps $1, \dots, m-1$. The inner calculation is now effectively advanced at timestep $\Delta t/M$, and the number of substeps M can be selected to be large enough to maintain the accuracy of the vorticity source and the stability of the algorithm used to calculate $\mathbf{x}(t)$. If t_o is the time spent, per timestep, on performing the outer calculation, then it is easy to show⁶ that factorisation of the source term yields a time saving of $(M-1)t_o$ per timestep over a computation where the rate of advance is limited by the inner calculation.

The inner aerodynamic model is constructed to be consistent with the blade element model used in the basic rotor-fuselage model. The spanwise variation of loading, and the rate of change of loading with time on each blade results in a source of vorticity into the flow. The source of vorticity from each blade is mapped onto an interpolating surface representing the (convected) trajectory of the blade during the current timestep, and the vorticity source $[S]_m^{n*}$ is obtained by transferring the vorticity from the interpolating surface into the computational domain by integration over the intersection between the interpolation surface and each of the computational cells.

A result illustrating the performance of the new wake model is presented in Figure 2. Figure 2a shows the model's prediction of the loading generated on the blades of Caradonna and Tung's¹⁶ two-bladed rotor in hover. Rapid convergence of the numerical solution, as the grid resolution is increased, to good agreement with experiment is shown. Figure 2b shows vorticity contours on an axial slice through the rotor wake. The vortex core positions show good agreement with the correlations obtained by Kocurek and Tangler,¹⁷ once the spatial resolution of the wake structure becomes sufficient to resolve the positions of individual vortex cores. In addition, the observed instability in the rotor wake, occurring after approximately two rotations of the rotor, shows that the present approach would appear to model, at least qualitatively, some of the unsteady dynamics and instability of the hovering rotor's far-wake reported by Leishman and Bagai.¹⁸

3 Flight Dynamic Application

Figure 3a shows an illustrative wake structure, visualised by plotting a series of surfaces on which the vorticity has constant magnitude, generated by the new model for the DERA AS330 Research Puma aircraft¹⁹ in trim at a forward flight speed of 30 knots. Of particular interest is the complexity of the wake structure generated by the new approach and the evident ability of the new model to capture some of the effects on the wake of the interaction between the main and tail rotors.

Figure 3b shows a comparison between the azimuthal variation of angle of attack for the Puma at a forward flight speed of 100 knots, calculated using both the dynamic inflow model and the vorticity transport model, and the flight data extracted by Padfield.¹⁹ Clearly visible in the experimental data is the ridge corresponding to interaction with the tip vortex shed from the previous blade, while a secondary interaction somewhat further inboard is less easily discernible. These interactive features are well-represented by the vorticity transport model, but are entirely absent from the simulation using the dynamic inflow model.

These results show that the vorticity transport model is indeed capable of introducing some of the real flowfield effects omitted by a low-order dynamic inflow formalism. The influence of the inclusion of these effects on the prediction of the flight dynamic behaviour of the aircraft is shown in Figure 4, where simulations incorporating the Peters dynamic inflow model and the vorticity transport model, and flight test data obtained on the DERA Research Puma, are compared.

Apart from the obvious deficiency in the modelling of the overall drag on the vehicle at high speed, which manifests itself as an underprediction of the required main rotor collective pitch, and consistent behaviour of the lateral cyclic pitch, longitudinal flapping and tail rotor collective pitch at speeds above about 80 knots, the most striking feature of the results presented here is the remarkable similarity in the predictions of the two induced velocity models throughout the speed range. There are two possible explanations for this interesting observation. The first is that the interactive features captured by the vorticity transport model have little impact on the modelling of main rotor trim throughout the speed range. Note though that where aerodynamic interactions are known to play an important role, such as in the tail rotor collective pitch, the predictions obtained using the vorticity transport model compare significantly better with flight data (at least over the range of validity of the airframe aerodynamic model) than do the predictions of the dynamic inflow model. This suggests the more plausible explanation for the observed similarities between the two models that the present rotor dynamic model, regardless of the induced velocity model being used, is relatively insensitive to the detailed structure of the loading distribution on the rotors. This argument has the obvious corollary that the primary deficiency in the predictive capabilities of the model must lie elsewhere than in the modelling of the rotor wake. In particular, the limitations of the rigid-blade model for the dynamics of the rotor, even for rotors with relatively stiff, articulated, blades, should perhaps be called into question. This

stands to reason since the close agreement between the predictions obtained using the dynamic inflow model and the vorticity transport model could feasibly result from the fact that the dynamic inflow model and the rigid-blade dynamic equations are both sensitive only to the zero'th and first moments of the radial distribution of the loading on the rotors. Incorporation of an aeroelastic model which allows the rotor to respond to the higher order moments of the loading distribution, such as those contained within the more detailed description of the blade loading inherent in the vorticity transport model, may start to show a more marked separation between the predictions of the two different induced velocity models, and indeed may help to improve the correlation between the model and flight-measured lateral cyclic pitch.

Comparison of the classical six-degree of freedom stability and control derivatives is presently compromised by an incomplete and inconclusive database for the full-scale Puma.²⁰ In Table 2 we present preliminary predictions of some of the more important derivatives, and compare against values identified at Glasgow University.²⁰ Standard deviations of the identified derivatives are given in parentheses. In all cases significant separation between the predictions of the dynamic inflow model and the vorticity transport model is seen, and arguably the predictions of the vorticity transport model bear closer relationship to the identified values, except in the case of the control derivative $L_{\theta_{1s}}$, where the large standard deviation suggests that the derivative was poorly identified from the flight data. Of particular note is the good agreement with the identified value of the vorticity transport model's prediction of M_v , a derivative estimated with high confidence from the flight data and of particular importance to the of the Puma's characteristic pitch response to Dutch roll.²⁰

Table 2. Stability and Control Derivatives (80 knots)

derivative	dynamic inflow	vorticity transport	flight identified ²⁰
M_v	0.004	-0.022	-0.021 (0.0015)
L_q	0.638	0.509	0.420 (0.0762)
M_p	-0.152	-0.103	-0.035 (0.0237)
$L_{\theta_{1s}}$	-2.904	-4.256	-2.822 (0.9620)
$M_{\theta_{1c}}$	2.327	4.512	- (-)

4 Conclusion

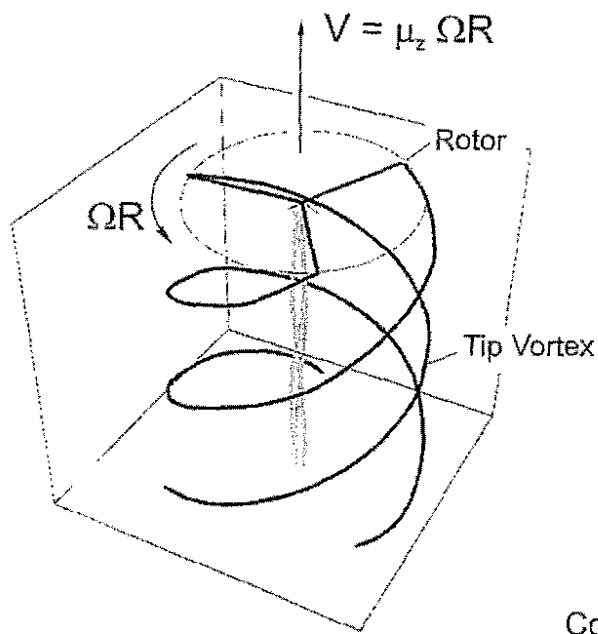
The primary objective of this Paper was to examine the significance of the incorporation of real flowfield effects, such as blade-vortex interaction and main rotor- tail rotor interaction, on the prediction of the flight mechanics of helicopters. Previous work had suggested that the omission of such effects in low-order dynamic inflow representations of the rotor wake was largely responsible for the discrepancies between the predictions of typical coupled rotor-fuselage models and flight experiments. The results presented here for the trimmed condition of the Puma main rotor show little sensitivity to the type of induced velocity model used in the simulation, but other results indicate the real flowfield effects indeed to be important. Together these observations suggest that the improved realism conferred by a high-resolution wake

model may not be fully evident in rotorcraft simulations without a simultaneous increase in fidelity of the rotor dynamic model.

5 Acknowledgements

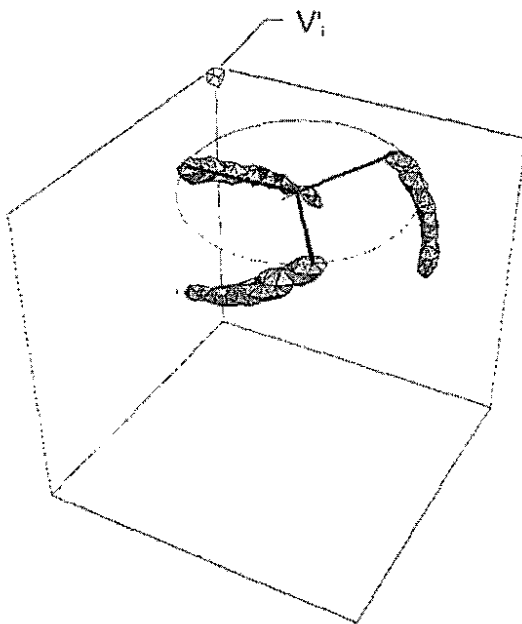
The research leading to this paper was conducted under the ongoing EPSRC grant GR/L 19614.

1. Chen, R.T.N., A Survey of Nonuniform Inflow Models for Rotorcraft Flight Dynamics and Control Applications, *Vertica*, Vol. 14, No. 2, 1990, pp. 147-184.
2. Houston, S.S. and Tarttelin, P.C., Validation of Mathematical Simulations of Helicopter Vertical Response Characteristics in Hover, *Journal of the American Helicopter Society*, Vol. 36, No. 1, 1991, pp. 45-57.
3. Padfield, G.D. and DuVal, R.W., Application Areas for Rotorcraft System Identification Simulation Model Validation, AGARD LS138, 1991, pp. 12.1-12.39.
4. Rosen, A. and Isser A., A Model of the Unsteady Aerodynamics of a Hovering Helicopter Rotor that Includes Variations of the Wake Geometry, *Journal of the American Helicopter Society*, Vol. 40, No. 3, 1995, pp. 6-16.
5. Peters, D.A. and HaQuang, N., Dynamic Inflow for Practical Applications, *Journal of the American Helicopter Society*, Vol. 33, No. 4, 1988, pp. 64-68.
6. Brown, R.E., Rotor Wake Modelling for Flight Dynamic Simulation of Helicopters, *AIAA Journal*, in press.
7. Houston, S.S., Validation of a Non-linear Individual Blade Rotorcraft Flight Dynamics Model Using a Perturbation Method, *The Aeronautical Journal*, Vol. 98, No. 977, 1994, pp. 260-266.
8. Houston, S.S., Validation of a Blade-Element Helicopter Model for Large-Amplitude Manoeuvres, *The Aeronautical Journal*, Vol. 101, No. 1001, 1997, pp. 1-7.
9. Houston, S.S., Validation of a Rotorcraft Mathematical Model for Autogyro Simulation, submitted to *Journal of Aircraft*.
10. Brown, R.E., Numerical Solution of the Two-Dimensional Navier Stokes Equations using Viscous-Convective Operator Splitting, MSc Thesis, College of Aeronautics, Cranfield Institute of Technology, Cranfield MK43 OAL, United Kingdom, 1990.
11. Schumann, U. and Sweet, R.A., A Direct Method for the Solution of Poisson's Equation with Neumann Boundary Conditions on a Staggered Grid of Arbitrary Size, *Journal of Computational Physics*, Vol. 20, No. 2, 1976, pp. 171-182.
12. Quackenbush, T.R., Boschitsch, A.H., and Wachspress, D.A., Fast Analysis Methods for Surface-Bounded Flows with Applications to Rotor Wake Modelling, *Proceedings of the American Helicopter Society 52nd Annual Forum*, Washington, 1996, pp. 1514-1531.
13. Toro, E.F., A Weighted Average Flux Method for Hyperbolic Conservation Laws, *Proceedings of the Royal Society of London, Series A: Mathematical and Physical Sciences*, Vol. 423, No. 1864, 1989, pp. 401-418.
14. Billett, S.J and Toro, E.F., On WAF-Type Schemes for Multidimensional Hyperbolic Conservation Laws, *Journal of Computational Physics*, Vol. 130, No. 1, 1997, pp. 1-24.
15. Toro, E.F., *Riemann Solvers and Numerical Methods for Fluid Dynamics : A Practical Introduction*, 2nd edition, Springer-Verlag, New York, 1999.
16. Caradonna, F.X. and Tung, C., Experimental and Analytical Studies of a Model Helicopter Rotor in Hover, *Vertica*, Vol. 5, No. 2, 1981, pp. 149-161.
17. Kocurek, J.D. and Tangler, J.L., A Prescribed Wake Lifting Surface Hover Performance Analysis, *Journal of the American Helicopter Society*, Vol. 22, No. 1, 1977, pp. 24-35.
18. Leishman, J.G. and Bagai, A., Challenges in Understanding the Vortex Dynamics of Helicopter Rotor Wakes, *AIAA Journal*, Vol. 36, No. 7, 1998, pp. 1130-1140.
19. Padfield, G.D., *Theoretical Modelling for Helicopter Flight Dynamics: Development and Validation*, ICAS-88-6.1.3, 1988, pp. 165-177.
20. Padfield, G.D., SA 330 Puma Identification Results, AGARD LS178, 1991, pp. 10.1-10.38.

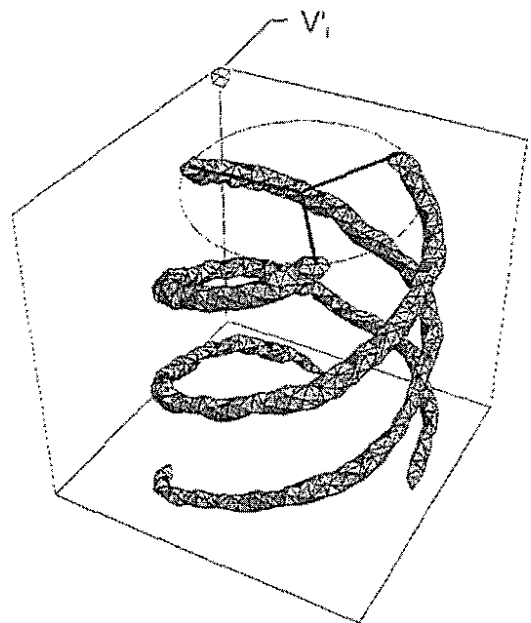


$$\begin{aligned} \mu_z &= 0.35 \\ C_T &= 0.088 \\ \sigma &= 0.1 \end{aligned}$$

Computational cell V_i is the smallest resolveable feature in the flow.



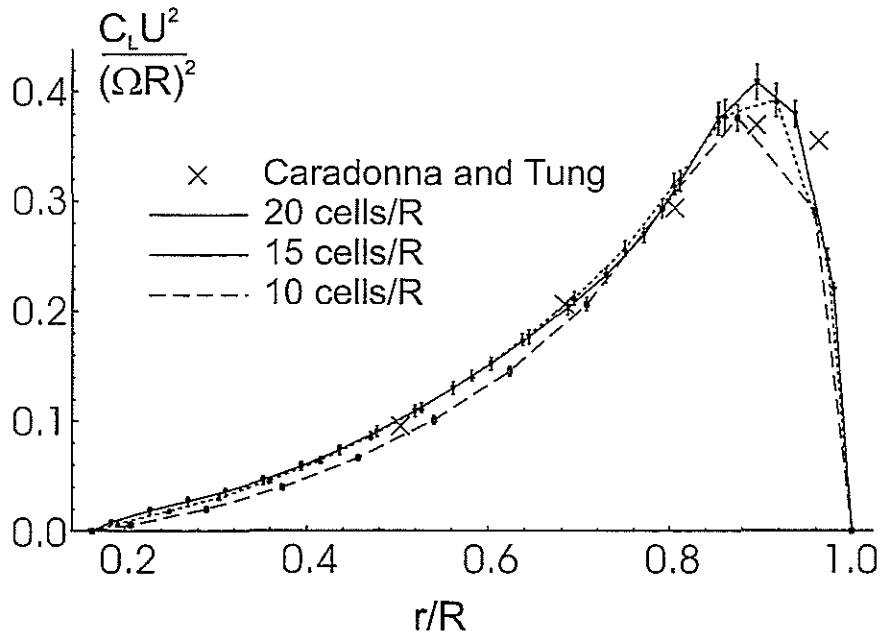
(a)
MIN-type Flux Limiter



(b)
SUPER-type Flux Limiter

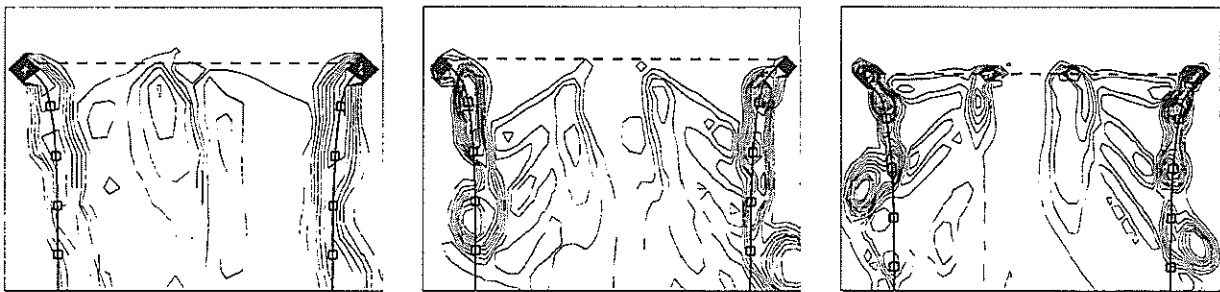
Figure 1. Vorticity Confinement Using Flux Limiting Functions.

(a) Blade Loading



Rotor TPP -----
 Kocurek and Tangler correlation:
 Wake Envelope _____
 Tip Vortex Position ◻

(b) Wake Structure

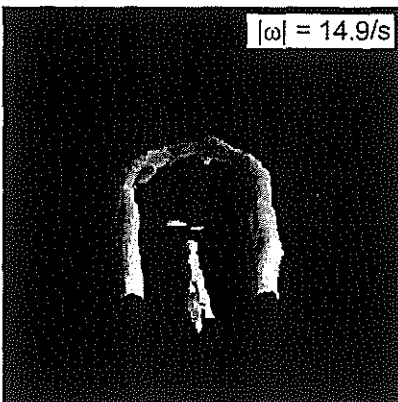
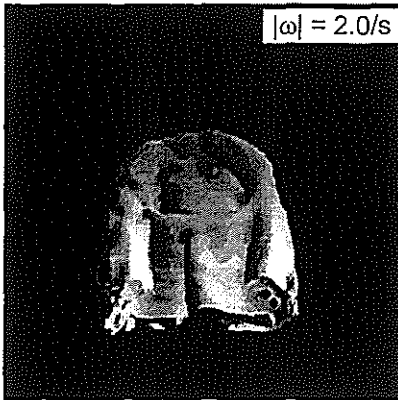
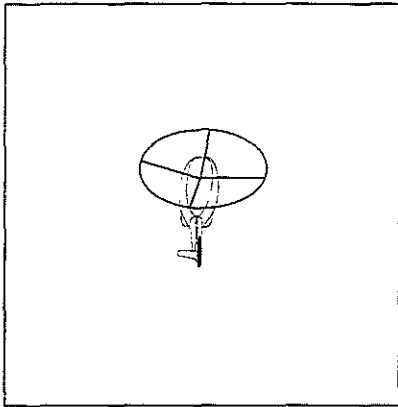


(a) 10 cells/R

(b) 15 cells/R

(c) 20 cells/R

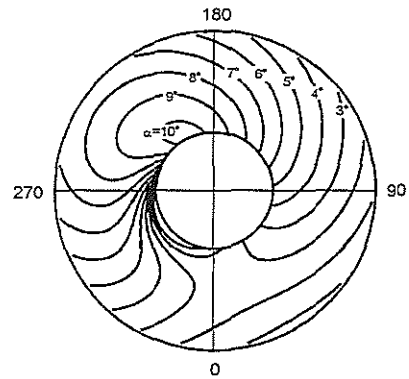
Figure 2. Blade Loading and Wake Structure for Caradonna and Tung's Hovering Rotor ($\theta_0 = 12.0^\circ$).



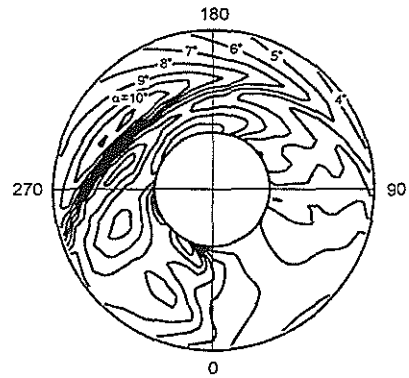
(a)
Vorticity Contours
30 Knots

AS330 PUMA
5805kg 3500ft

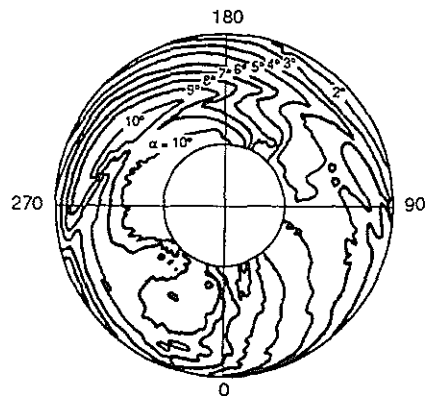
Dynamic Inflow Model



Vorticity Transport Model



Flight Measured



(b)
Blade Angle of Attack
100knots

Figure 3. Wake Geometry and Inflow Distribution for AS330 Puma.

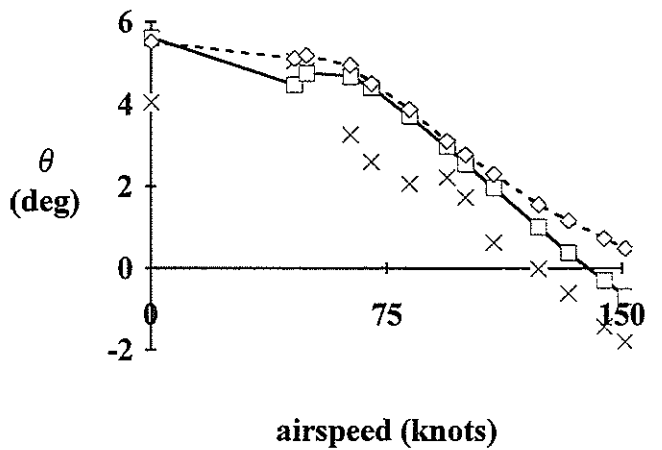
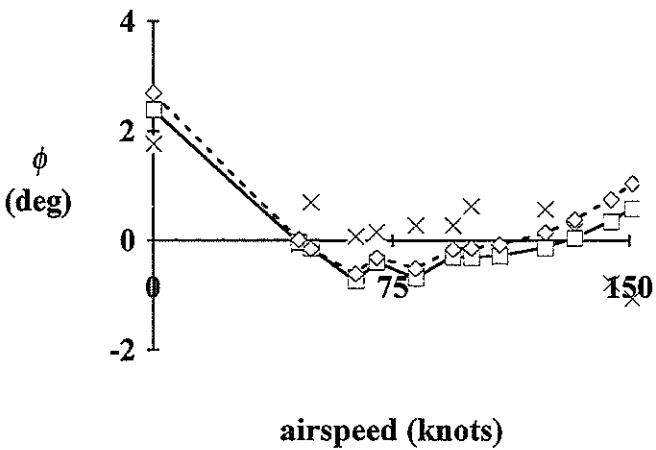
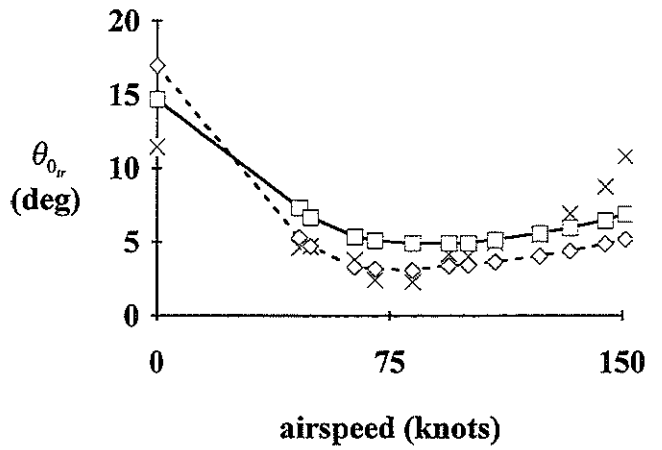
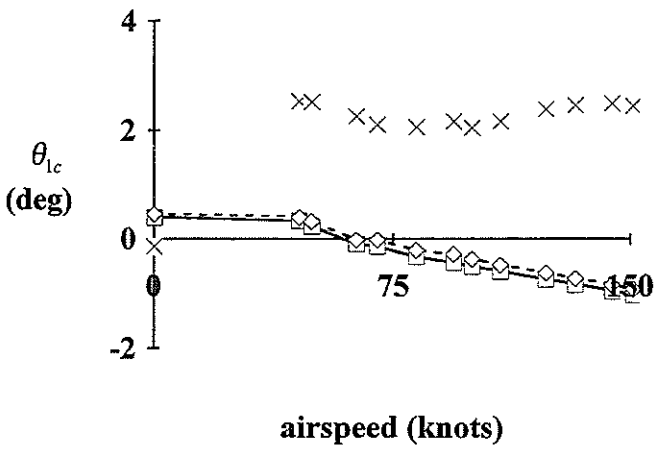
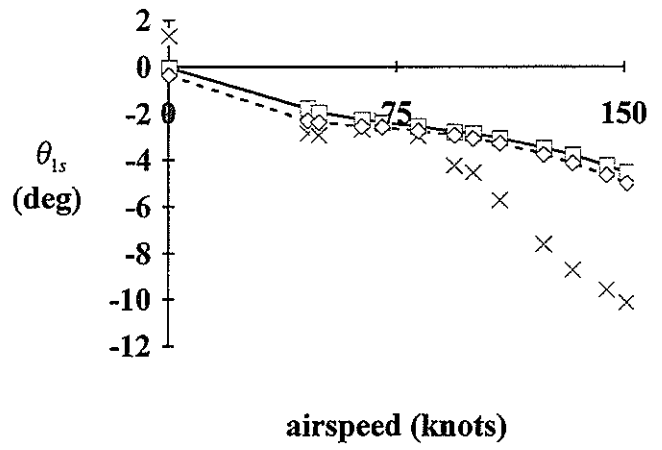
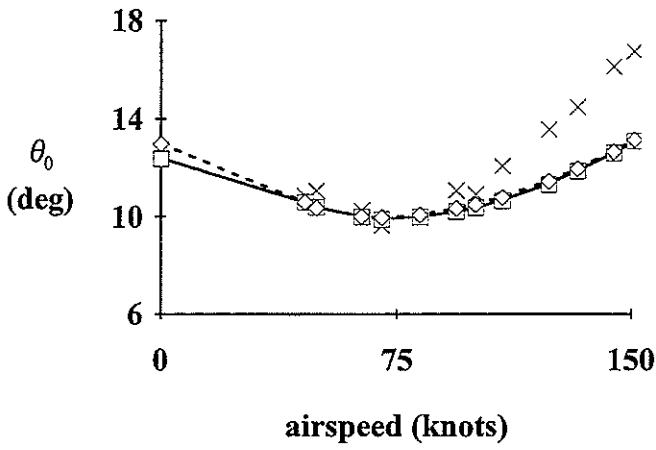
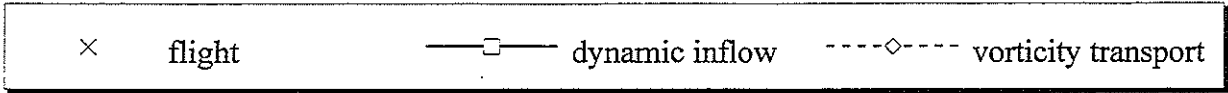


Figure 4. Variation of Trim States with Forward Speed for AS330 Puma.